JOURNAL OF PROPULSION AND POWER
Vol. 10, No. 2, March–April 1994

Forcing Function Generator Fluid Dynamic Effects on Compressor Blade Gust Response

Kuk H. Kim* and Sanford Fleeter†
Purdue University, West Lafayette, Indiana 47907

To investigate the fundamental flow forcing function phenomena generating different blade row gust responses, in particular attached and separated flow forcing functions, a series of experiments are performed in an extensively instrumented axial flow research compressor. In these experiments, the gust ratio magnitude is controlled without affecting the forcing function fluid dynamics, i.e., attached or separated flow, thereby enabling a controlled study of the effect of steady loading. Periodic 2-E unsteady aerodynamic forcing functions to the first stage rotor are generated by fundamentally equivalent honeycomb sections and flat plate airfoils, with unsteady linear theory gust requirements considered. Then the resulting rotor blade row gust response is measured over a range of steady loading levels and the gust response data correlated with the appropriate linear theory predictions. These experiments show that the forcing function generator fluid dynamics is significant with regard to the resulting unsteady aerodynamic gust response. Also demonstrated is the decreased correlation of the gust response data with linear theory predictions as the steady loading is increased.

Nomenclature

$C_{p,ps}$ = pressure surface complex unsteady pressure coefficient
$C_{p,ss}$ = suction surface complex unsteady pressure coefficient
$\bar{C}_{pi}$ = steady pressure coefficient at ith chord position
$\bar{C}_{p,p}$ = pressure surface steady pressure coefficient
$\bar{C}_{p,s}$ = suction surface steady pressure coefficient
$\bar{C}_l$ = steady lift coefficient
i = rotor relative flow incidence angle
$\bar{i}$ = mean rotor relative flow incidence angle
k_1 = streamwise wave number, reduced frequency
k_2 = transverse wave number
$\bar{P}_{exit}$ = static pressure at rotor exit
p_1' = first harmonic of Fourier decomposed pressure
U = flow velocity or wheel speed
u = streamwise gust component
u^+ = first harmonic streamwise gust component
u^+/v^+ = streamwise to transverse gust ratio
$\bar{V}_x$ = mean axial velocity
v = transverse gust component
v^+ = first harmonic transverse gust component
$\bar{W}$ = mean rotor relative velocity
w = instantaneous rotor relative velocity
x_1 = first chordwise position for blade surface steady pressure measurement
x_2 = last chordwise position for blade surface steady pressure measurement
α = absolute flow angle
$\bar{\alpha}$ = mean absolute flow angle
β = rotor relative flow angle
$\bar{\beta}$ = mean rotor relative flow angle
ΔC_p, $C_{\Delta p}$ = complex unsteady pressure difference coefficient
$\Delta \bar{C}_p$ = steady pressure difference coefficient

Presented as Paper 93-0157 at the 31st Aerospace Sciences Meeting, Reno, NV, Jan. 11–14, 1993; received April 19, 1993; revision received Aug. 24, 1993; accepted for publication Sept 9, 1993.

*AFRAPT Trainee, School of Mechanical Engineering.
†Professor, School of Mechanical Engineering.

Introduction

THE spatial flow nonuniformities generated by inlet guide vanes, stators vanes, and struts are periodic temporal variations to downstream rotor blades. These spatial flow nonuniformities in the stationary frame of reference are sources of periodic excitation to the rotor blades. When the frequency of these periodic flow nonuniformities coincides with a blade natural frequency, fatigue failure of the rotor blade may result, thereby compromising engine durability.

The prediction of the flow-induced vibratory response of a blade row first requires a definition of the unsteady aerodynamic forcing function in terms of its harmonics, with each harmonic independently considered. Thus, even though forcing functions may be generated by a wide variety of fundamentally different sources, the forcing functions are assumed to be equivalent if their harmonics are the same. The unsteady aerodynamic response of the blade row to each forcing function harmonic is then assumed to be comprised of two components: the disturbance being swept past the nonresponding airfoils, termed the gust unsteady aerodynamic and the airfoil vibratory response to this disturbance, referred to as the motion-induced unsteady aerodynamics or the aerodynamic damping.

Early treatments of unsteady flow due to periodic gusts were developed in the linear approximation wherein the mean flow is assumed to be uniform. In this approximation, the steady and unsteady flowfields are completely uncoupled from one another, with the upstream generated periodic gust aerodynamic forcing functions convected with the uniform mean flow. Semianalytical unsteady aerodynamic analyses based on this linear model have been developed for cascades in subsonic and supersonic flows.[1–4] Such models are currently being extended to consider unsteady flows linearized about a nonuniform mean flow, with the gust interacting with the mean flow.[5–7]

A number of experiments have been directed at the verification of such mathematical models and the determination of their applicability and limitations. As a generalization, it appears that if the assumptions inherent in these analyses are modeled, then the experiments provide data which are in

Table 1 Overall airfoil and compressor characteristics

	IGV	Rotor	Stator
Airfoil type	C4	C4	C4
Number of airfoils	36	43	31
Chord, C, mm	30	30	30
Solidity, C/S	0.96	1.14	0.822
Camber, q	36.9	28.0	27.7
Stagger angle, g	21.0	36.0	−36.0
Inlet metal angle, β_1	0.0	50.0	30.0
Aspect ratio	2.0	2.0	2.0
Thickness/chord, %	10.0	10.0	10.0
Axial spacing (%C)	IGV/R = 0.63	R/S = 0.55S/R = 0.38	——
Reynolds number × 10^{-5} (based on chord)	5.0	6.3	6.3
Flow rate, kg/s	——	2.03	——
Design axial velocity, m/s	——	24.4	——
Design rotational speed, rpm	——	2250	——
Number of stages	——	3	——
Design stage pressure ratio	——	1.0	——
Inlet tip diameter, mm	——	420	——
Hub/tip radius ratio	——	0.714	——
Stage efficiency, %	——	85	——

agreement with the predictions. However, if actual compressor operating conditions, i.e., finite camber, steady loading, and nonzero incidence angle, are experimentally modeled, then the data-prediction correlations are not nearly as good.

Of particular interest herein are the experiments performed by Manwaring and Fleeter,[8] which investigated the unsteady aerodynamic response of a rotor blade row to two classically equivalent forcing functions, as defined by linear theory. Their data first revealed the dependency of the unsteady aerodynamic response to a particular forcing function.

Later, Kim and Fleeter[9] identified the importance of the gust generator fluid dynamics on the resulting blade row response. Their data attributed the differences in the gust response of the 2 per rotor revolution or 2-E inlet distortion and flat plate wakes of Manwaring and Fleeter[8] to the fluid dynamics of the gust generators. Namely, the inlet distortion gust was generated by an attached flow gust, while the flat plate gust was due to a separated flow gust. However, in these experiments, a controlled study of the effect of steady loading could not be performed because of the particular forcing function generators, i.e., the gust ratio magnitude, u^+/v^+, could not be controlled without affecting the forcing function fluid dynamics.

In this article, the fundamental forcing function phenomena fluid dynamics generating different blade row gust responses are investigated in a controlled manner, including the important effects associated with the forcing function gust magnitude. This is accomplished by means of a series of experiments directed at the investigation of unsteady aerodynamic blade row response to gusts generated by attached and separated flow fluid dynamics from nonairfoil shape gust generators. With these gust generators, the gust ratio magnitude can be controlled without affecting the forcing function fluid dynamics, i.e., attached or separated flow, thereby enabling a controlled study of the effect of steady loading.

Periodic 2 per rotor revolution or 2-E unsteady aerodynamic forcing functions to the first-stage rotor row of the extensively instrumented Purdue Axial Flow Research Compressor are generated by two honeycomb sections and flat plates installed in the compressor inlet. These forcing functions are measured with a rotating cross hot-wire, with the resulting blade row unsteady aerodynamic gust response measured with dynamic pressure transducers embedded in the blade for steady loading levels ranging from −3 to 6 deg. Furthermore, unsteady linear theory gust requirements are considered, with appropriate gust response data correlated with predictions from the subsonic unsteady aerodynamic flat plate cascade analysis of Smith.[10]

Research Compressor

The Purdue Axial Flow Research Compressor models the fundamental turbomachinery unsteady aerodynamic multistage interaction phenomena, which include the incidence angle, the velocity and pressure variations, the aerodynamic forcing function waveforms, the reduced frequency, and the unsteady blade row interactions. The compressor is driven by a 15 hp dc electric motor at a speed of 2250 rpm. Each identical stage contains 43 rotor blades and 31 stator vanes having a British C4 airfoil profile, with the first stage rotor inlet flowfield established by an inlet guide vane (IGV) row of 36 airfoils. The 2-E unsteady aerodynamic forcing functions are generated by two honeycomb sections and flat plates installed 180-deg apart in the compressor inlet. The overall compressor and airfoil characteristics are defined in Table 1.

The compressor aerodynamic performance is determined utilizing a 48-port Scanivalve system, thermocouples, and a venturi orifice to measure the required pressures, temperatures, and flow rate, respectively. The Scanivalve transducer is calibrated each time data are acquired, thus automatically compensating for zero and span shifts of the transducer output. A 95% confidence interval, rms error analysis of 20 samples is performed for each steady data measurement.

Instrumentation

Both steady and unsteady rotor blade row data are obtained. The steady data quantify the rotor row mean inlet flowfield and the resulting rotor blade midspan steady loading distribution. The unsteady data define the periodic aerodynamic forcing function and the resulting midspan blade surface periodic unsteady pressure distributions.

The inlet flowfield, both steady and unsteady, is measured with a rotating cross hot-wire probe. The inlet flowfield of the first-stage rotor row is measured in the rotating frame of reference by mounting the hot wire on the rotor drum 18.8% chord upstream and 65% blade spacing from a rotor blade, depicted in Fig. 1. The hot wire is oriented for maximum sensitivity, achieved when the 0-deg flow incidence corresponds to the position at which the flow angle is 45 deg to both wires. The hotwire is calibrated for velocities from 21.3 to 62.5 m/s and ±40-deg flow angle variations. The uncertainties in the velocity and the flow angle measurements were determined to be 5% and ±0.5 deg. Centrifugal loading ef-

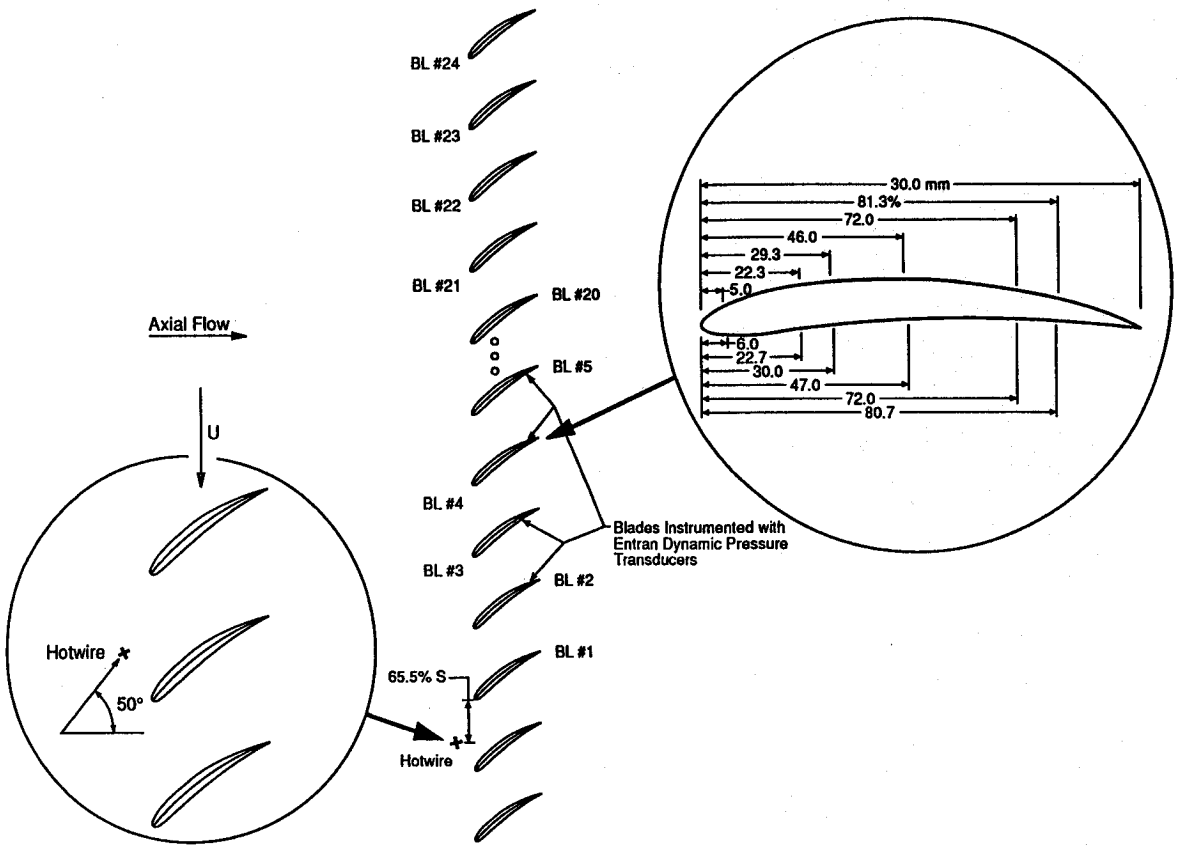

Fig. 1 Rotor instrumentation.

fects on the rotating hot-wire sensor resistances and thus the responses were found to be negligible.

The detailed steady aerodynamic loading on the rotor blade surfaces is measured with a chordwise distribution of 20 midspan static pressure taps, 10 on each surface. The static pressure at the rotor exit plane, measured with a rotor drum static tap, is used as the blade surface static pressure reference. These static pressure measurements are made using a rotor based, 48-port constant speed drive Scanivalve system located in the rotor drum.

The measurement of the midspan rotor blade surface unsteady pressures is accomplished with 20 ultraminiature, high-response transducers embedded in the rotor blades at the same chordwise locations as the static pressure taps. To minimize the possibility of flow disturbances associated with the inability of the transducer diaphragm to exactly maintain the surface curvature of the blade, a reverse mounting technique is utilized. The pressure surface of one blade and the suction surface of the adjacent blade are instrumented, with transducers embedded in the nonmeasurement surface and connected to the measurement surface by a static tap. The embedded dynamic transducers are both statically and dynamically calibrated. The static calibrations show good linearity and no discernible hysteresis. The dynamic calibrations demonstrate that the frequency response, in terms of gain attenuation and phase shift, are not affected by the reverse mounting technique. The maximum error in gain and phase angle were determined to be 0.60 dB and 1.5 deg, respectively.

The rotor-based static pressure Scanivalve transducer, rotating cross hot-wire probe and 20 blade surface dynamic pressure transducers are interfaced to the stationary frame-of-reference through a 40-channel slip-ring assembly. On-board signal conditioning of the transducer output signals is performed to maintain a good signal-to-noise ratio through the slip rings. The remaining 17 channels of the slip-ring assembly are used to provide excitation to the transducers and on/off switching to the Scanivalve dc motor.

Data Acquisition and Analysis

Steady Pressure Data

The rotor blade surface static pressure data are defined by an rms error analysis of 20 samples with a 95% confidence interval. The airfoil surface static pressures are presented in terms of a nondimensional steady pressure coefficient, with the steady lift coefficient calculated by integrating the differential steady pressure coefficient across the rotor blade chord:

$$\bar{C}_{p,i} = \frac{\bar{P}_i - \bar{P}_{\text{exit}}}{\rho \bar{W}^2} \tag{1}$$

Since the blade surface and the reference static pressures are measured at different radii, a correction is applied to the exit steady pressure to account for centrifugal effects.[8] The uncertainty in the steady pressure coefficient was estimated to be $\pm 5.6\%$.

Periodic Data

The periodic data of interest are the harmonic components of the aerodynamic forcing function to the first stage rotor blade row, together with the resulting rotor blade surface unsteady pressures and unsteady pressure differences. These are determined by defining a digitized ensemble-averaged periodic unsteady aerodynamic data set consisting of the rotating cross hot-wire probe and blade surface dynamic pressure transducer signals at each steady operating point. In particular, these time-variant signals are digitized with a high-speed analog-digital (A-D) system at a rate of 20 kHz and then ensemble averaged.

The key to this averaging technique is the ability to sample data at a preset time, accomplished by an optical encoder mounted on the rotor shaft. The microsecond range step voltage signal from the encoder is the data initiation time reference and triggers the high-speed A-D multiplexer system. To significantly reduce the random fluctuations superimposed on

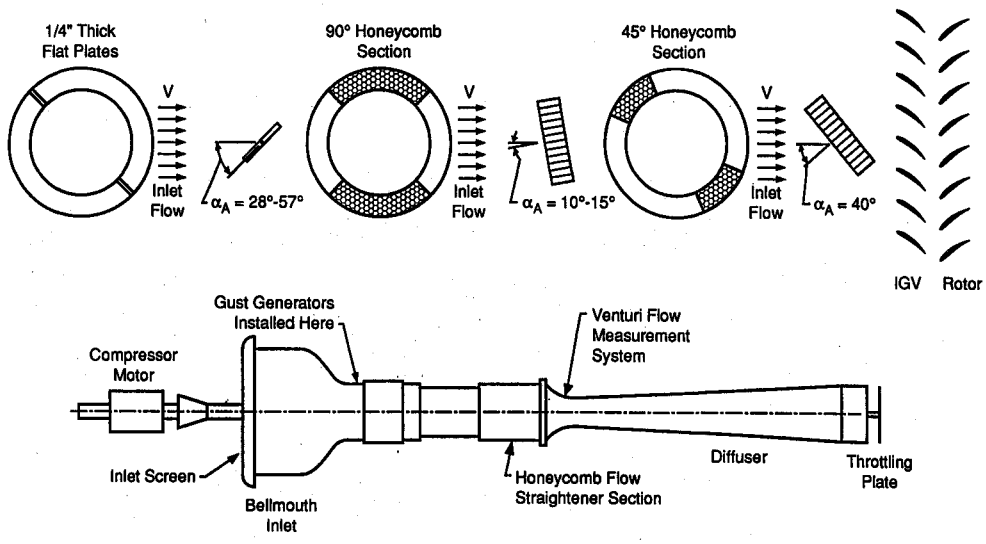

Fig. 2 Facility and gust generators.

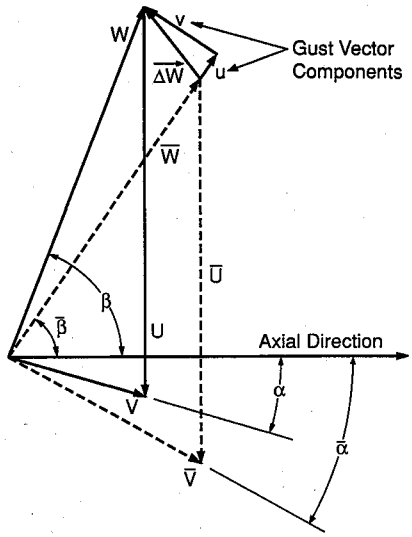

Fig. 3 Decomposition of rotor inlet velocity: ——, instantaneous velocity triangle; -----, mean velocity triangle.

the periodic signals of interest, 200 averages are used. A fast Fourier transform (FFT) algorithm is then applied to these ensemble-averaged signals to determine the harmonic components of the unsteady aerodynamic forcing function and the resulting rotor blade surface harmonic unsteady pressures and pressure differences. Since ensemble averaging adequately separates the major frequency components, no windowing functions are applied to the data during FFT.

Forcing Function

The 2-E unsteady aerodynamic forcing functions are generated by two honeycomb sections and flat plates installed 180 deg apart in the compressor inlet, as illustrated in Fig. 2. These forcing functions are broadly categorized as attached flow and separated flow. The forcing function to the first-stage rotor, the unsteady rotor inlet flowfield, is measured with the rotating cross hot-wire probe which quantifies the relative velocity and flow angle. To the rotor, the flow from the upstream honeycombs or flat plates appear as deficits in the rotor relative inlet velocity W and fluctuations in the rotor relative inlet flow angle. Therefore, the total flow consists of freestream and wake regions, with the instantaneous value of W increased in the wake region and decreased in the freestream. The total rotor inlet relative velocity gust ΔW is the vector difference between the instantaneous and mean relative velocity W. It has two components, u and v, parallel and

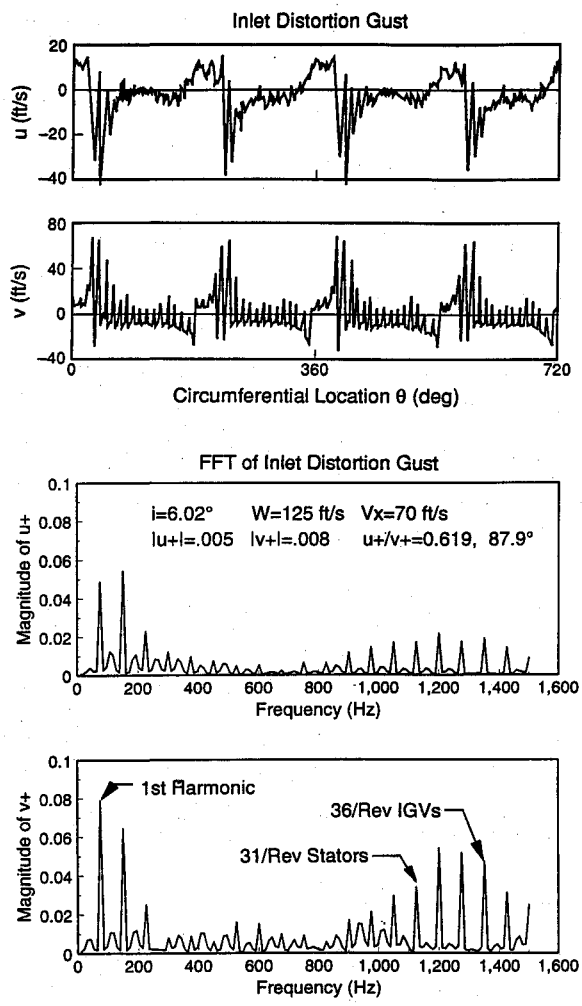

Fig. 4 Forcing function and streamwise and normal gust component FFT.

normal to the mean flow direction. The gust and its components are depicted in the velocity diagram of Fig. 3.

The fundamental frequency of interest is the 2-E forcing function frequency. Thus, an harmonic analysis is utilized in the data analysis, accomplished by taking the FFT of both the time variant rotor inlet flowfield and the resulting unsteady aerodynamic response of the first-stage rotor row, with only the components at the fundamental frequency or its harmonics analyzed. Figure 4 shows the streamwise and trans-

verse gust components and their FFT, with the u and v harmonics denoted by u^+ and v^+, and nondimensionalized by the mean rotor relative velocity. This Fourier transformed inlet flow, defined by u^+ and v^+, is the unsteady aerodynamic forcing function to the downstream rotor row.

Unsteady Pressure Data

The rotor blade pressure and suction surface unsteady pressure data are analyzed to determine the harmonics of the chordwise distribution of the unsteady pressure coefficient:

$$C_{p,i} = \frac{p_i^+}{\rho \bar{W}^2 v^+} \tag{2}$$

The unsteady differential pressure coefficient is determined by subtracting the unsteady pressure coefficient on the suction surface from that on the pressure surface. The uncertainty in the unsteady pressure coefficient was estimated to be ±6.7%. The resulting unsteady lift is calculated by integrating the unsteady differential pressure coefficient over the chord. Then the measured and predicted unsteady lift values are correlated by means of the unsteady lift ratio, with both the theoretical and experimental differential pressure coefficients integrated between the first and last chordwise positions of the experimental data:

$$L_{\text{corr}} = \frac{C_{l,\text{exp}}}{C_{l,\text{theory}}} = \frac{\frac{1}{c}\int_{x_1}^{x_2} \Delta C_{p,\text{exp}}\, dx}{\frac{1}{c}\int_{x_1}^{x_2} \Delta C_{p,\text{theory}}\, dx} \tag{3}$$

Note that if the experimental data are in exact agreement with the unsteady linear theory prediction, the unsteady lift ratio L_{corr} will have a magnitude of 1.0 and a phase angle of 0 deg.

Results

A series of experiments are performed in the Purdue Axial Flow Research Compressor to investigate in a controlled manner the fundamental forcing function fluid dynamics generating different blade row gust responses effects, i.e., attached or separated flow, as well as steady loading effects on the resulting gust response of the first-stage rotor row. Attached flow forcing functions are generated by 90-deg honeycomb sections at 5–15-deg angle of attack (AOA), with separated flow forcing functions resulting from flat plates at 28–57-deg AOA, and 45-deg honeycomb sections at 40-deg AOA. With these gust generators, the gust ratio magnitude could be controlled without affecting the forcing function fluid dynamics, i.e., attached or separated flow, thereby enabling a controlled study of the effect of steady loading.

For each forcing function flow, four steady loading conditions, as characterized by the rotor relative mean flow incidence angles are studied: $\bar{i} = -3$, 0, 3, and 6 deg. The magnitude and phase of u^+/v^+ as a function of loading for the 90- and 45-deg honeycombs and flat plates are shown in Fig. 5. At each steady loading, the magnitude of u^+/v^+ is held relatively constant at 0.80 for the 90-deg honeycombs and the flat plates and at 0.62 for the 45-deg honeycomb. However, the resulting phase of u^+/v^+ varies from 83 to 69 deg for the 90-deg honeycomb, from 96 to 88 deg for the 45-deg honeycomb, and from 59 to 63 deg with the flat plates.

Surface Steady Pressure Distributions

The chordwise rotor blade surface steady pressure distributions for the three forcing function flow types are presented in Fig. 6 for the low and high rotor steady loading levels, $\bar{i} = -3$ and 6 deg. These data are compared with predictions from an incompressible, inviscid small camber airfoil cascade

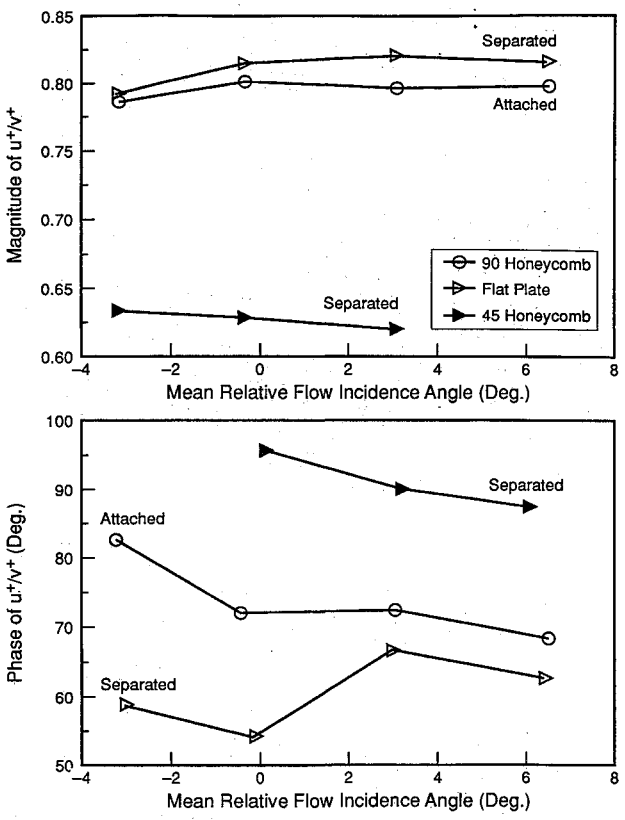

Fig. 5 Honeycomb and flat plate forcing functions.

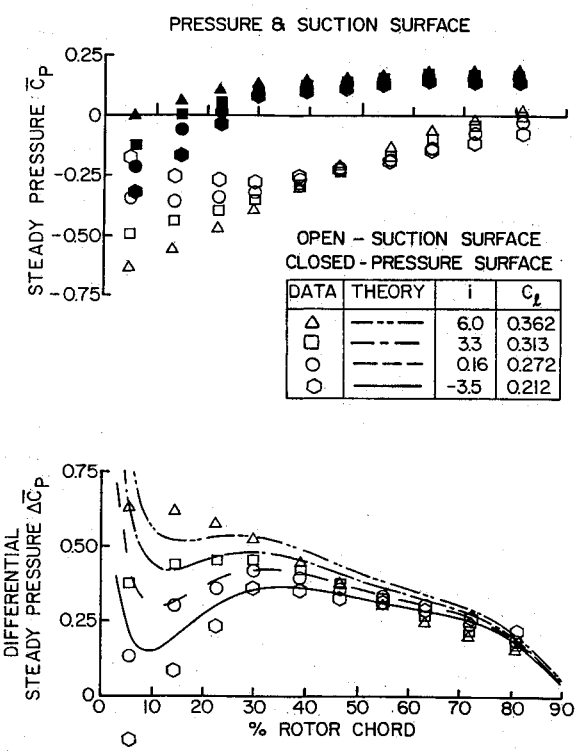

Fig. 6 Loading effect on rotor blade surface steady pressures.

analysis. The rotor blade surface steady pressure distribution is a function of the steady loading level, but independent of the forcing function.

In the pressure surface leading-edge region, the steady pressure coefficient increases with loading. It then increases until approximately 30% chord where it becomes constant, independent of the loading. In contrast, steady loading affects the suction surface over the entire chord, with the suction surface steady pressure coefficient a strong function of the steady

loading level. Note that there is no evidence of suction surface steady flow separation. With regard to the differential steady pressure coefficient, the leading-edge value is negative at negative values of the relative mean flow incidence, approximately zero at 0-deg incidence, increasing with increased loading. These data exhibit relatively good correlation with the predictions. The steady pressure data is accomplished by the mean rotor relative velocity measured with the rotor blades adjacent to the hot wire removed to determine the value of the mean rotor relative velocity $\bar{W}$.

Honeycomb and Flat Plate Attached and Separated Flow Generated Forcing Functions

Figure 7 shows the Fourier decomposition of the 90-deg honeycomb attached flow forcing function. The dominant u^+ magnitude occurs at the fundamental frequency with the higher harmonic magnitudes decreased. The v^+ spectrum also has a dominant v^+ magnitude at the fundamental frequency, with the higher harmonic magnitudes decreasing rapidly.

The Fourier decomposition of the flat plate generated separated flow forcing function spectrum is presented in Fig. 7. In contrast to the attached flow forcing function, the fundamental frequency u^+ magnitude does not dominate and the higher harmonics are an integral part of the entire spectrum. Similarly, no particular harmonic of v^+ dominates, and the magnitudes of all harmonics are large. In addition, there is a minimum v^+ harmonic.

The second separated flow forcing function is generated by the 45-deg honeycomb sections. The Fourier decomposition of this separated flow forcing function exhibits some differences as compared to the separated flow forcing functions generated by the flat plates (Fig. 7). The first two harmonics of u^+ dominate the spectrum, with the second harmonic being larger than the first, but the higher harmonics are of lower magnitude than the flat plate forcing function. The first three harmonics of v^+ and the harmonics near 1200 Hz are dominant in the v^+ spectrum, thereby producing a minimum v^+ harmonic, analogous to the flat plate separated forcing function.

These differences in the forcing function spectrum between the attached flow 90-deg honeycomb and the separated flow flat plates and 45-deg honeycomb are similar to the differences that resulted from changing the gust generating airfoil AOA from 5 to 20 deg,[9] i.e., the magnitudes of the higher harmonics increase with flow separation relative to the fundamental frequency value leading to a more impulsive forcing function when the flow generating the gust is separated. These results indicate that attached and separated flow forcing functions have key characteristics that do not depend on the particular

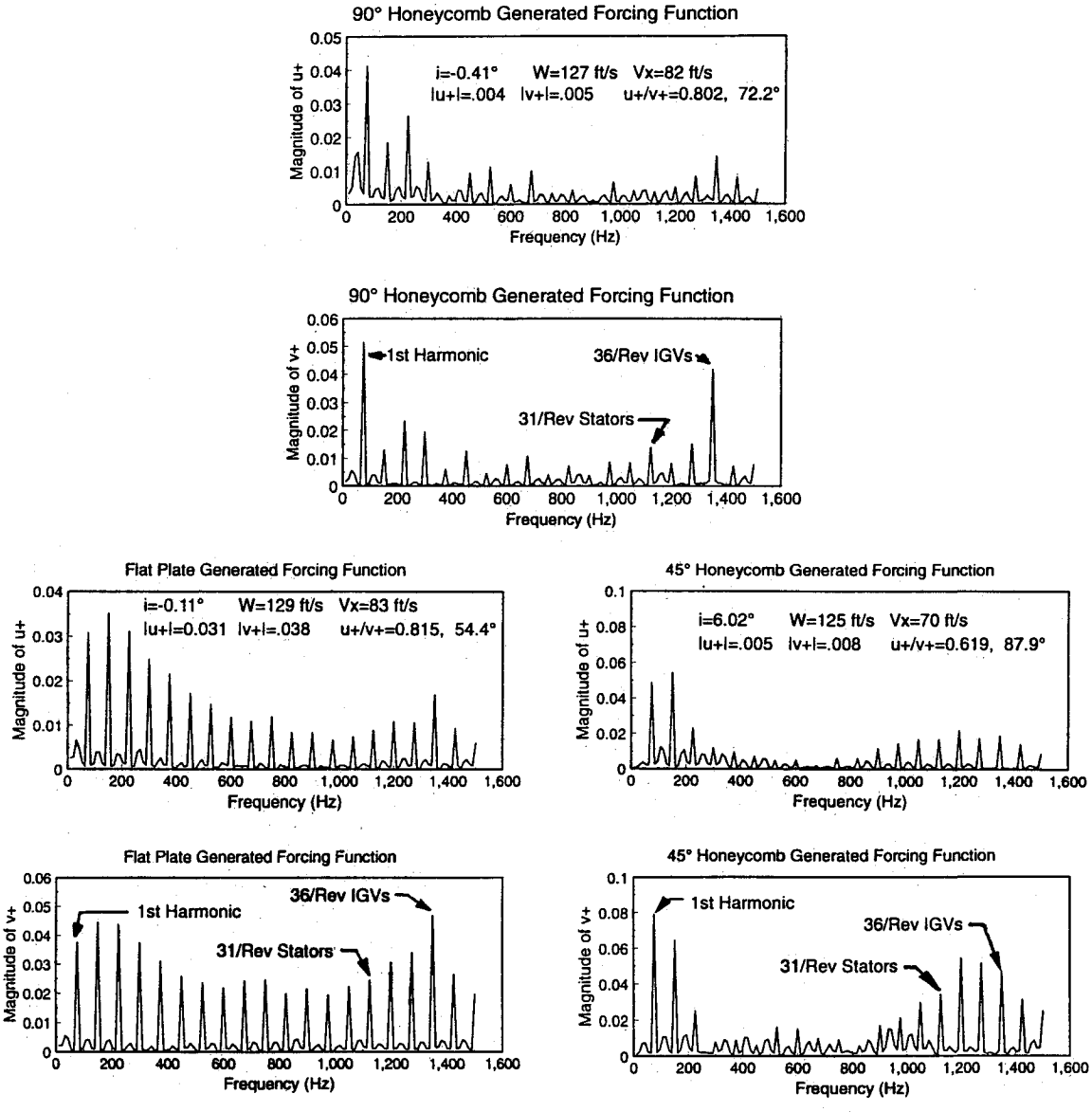

Fig. 7 FFT of forcing functions.

forcing function generator. Thus, the concept of attached and separated flow forcing functions is applicable to any gust generators exhibiting these key characteristics.

Forcing Function Generator Fluid Dynamic Effects on Gust Response

Pressure Surface

Figure 8 shows the pressure surface gust response from the 90-deg honeycomb attached flow generated forcing function. The magnitude data smoothly decrease with chord, becoming constant at approximately 20% chord, and have a small dependence on steady loading. The phase data are independent of steady loading and increase smoothly from the leading edge, becoming constant at approximately 40% chord.

The chordwise trends in the magnitude response data resulting from the flat plate and the 45-deg honeycomb separated flow generated forcing functions (Figs. 9 and 10) are generally the same as that of the 90-deg honeycomb attached flow generated response. However, the magnitude data from the flat plate separated flow generated forcing function are a stronger function of steady loading over the entire chord, with the 45-deg honeycomb separated flow generated response magnitude data independent of steady loading over the front 30% chord, then becoming a weak function of steady loading. In addition, the level of the magnitude data from the flat plate is smaller than that resulting from the attached flow 90-deg honeycombs and the separated flow 45-deg honeycombs, with the magnitude data levels generated by the honeycombs approximately the same.

The pressure surface phase response data are unchanged as the forcing function generator is altered from the 90-deg honeycombs with attached flow to the flat plates with separated flow and the 45-deg honeycombs with separated flow. In comparison to the pressure surface response data resulting from the NACA airfoil generated attached and separated flow forcing functions reported by Kim and Fleeter,[9] the 90-deg honeycomb attached flow response differs significantly. However, the flat plate and 45-deg honeycomb separated flow forcing function generated responses agree in trend with those of the airfoil generated separated flow forcing function. These results reveal that the pressure surface gust response resulting from the attached flow generated forcing functions is sensitive to the particular forcing function generator, but that the pressure surface gust response resulting from separated flow generated forcing functions is less sensitive to the particular wake generator.

Suction Surface

Altering the attached flow forcing function from that generated by the 90-deg honeycombs to the separated flow forcing functions generated by the flat plates and the 45-deg honeycombs has a significant effect on the resulting suction surface gust response (Figs. 11–13). With the attached flow generated forcing function, the gust response magnitude rapidly decreases in the leading-edge region, becoming somewhat constant between 20–40% chord, then decreasing to a minimum near 50% chord. Aft of 55% chord, there is a large increase followed by a sudden decrease. Also, these magnitude data are a function of steady loading near the leading edge and aft of 55% chord.

As the forcing function generator flowfield is changed to separated flow, the resulting chordwise trends in the suction surface gust response from both the flat plate and the 45-deg honeycomb are similar to the attached flow forcing function generated gust magnitude response. However, the chordwise distribution of the magnitude data become smoother with the magnitude data decreasing more rapidly in the leading-edge region. Also, the flat plate separated flow forcing function generated gust magnitude data at the leading edge show little effect from steady loading changes. Rather, these magnitude data are strongly influenced by steady loading between 10% chord and the trailing edge. The gust magnitude data generated by the separated flow 45-deg honeycomb have similar trends over the front 40% chord, but become less dependent on steady loading aft of 40% chord.

With regard to the suction surface phase response data, the 90-deg honeycomb generated gust phase response is independent of steady loading over the front 20% chord and decreases gradually with chord, becoming a function of steady

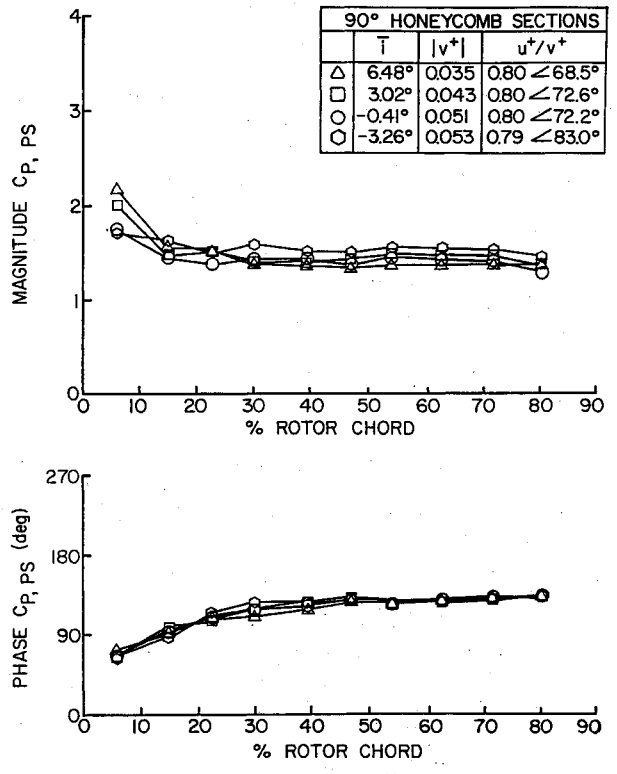

Fig. 8 Pressure surface 90-deg honeycomb attached flow generated gust response.

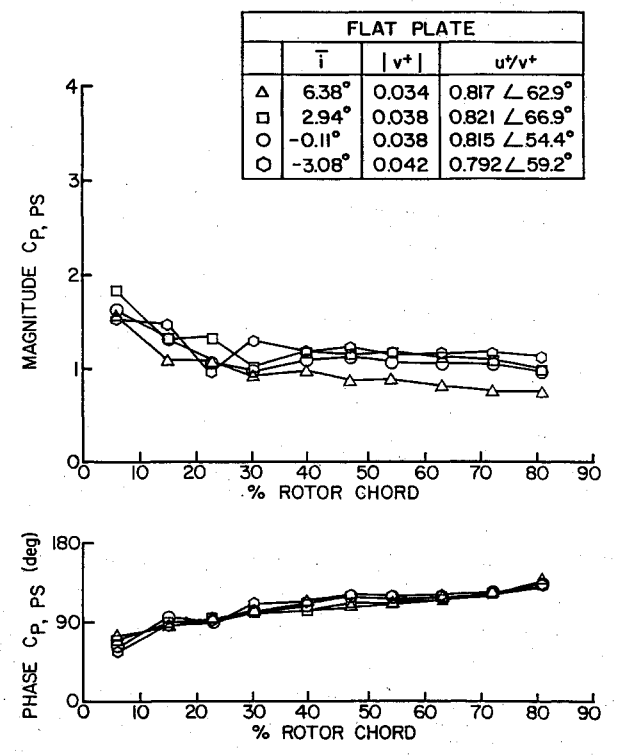

Fig. 9 Pressure surface flat plate separated flow generated gust response.

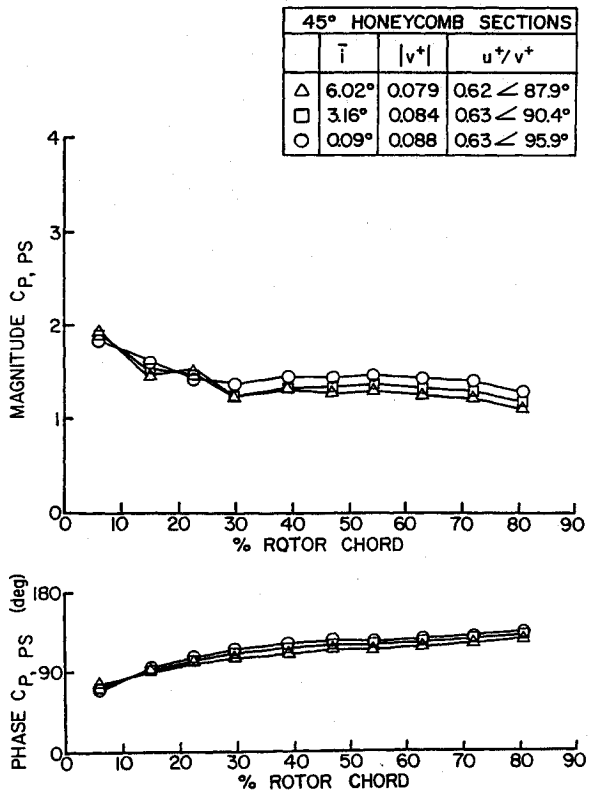

Fig. 10 Pressure surface 45-deg honeycomb separated flow generated gust response.

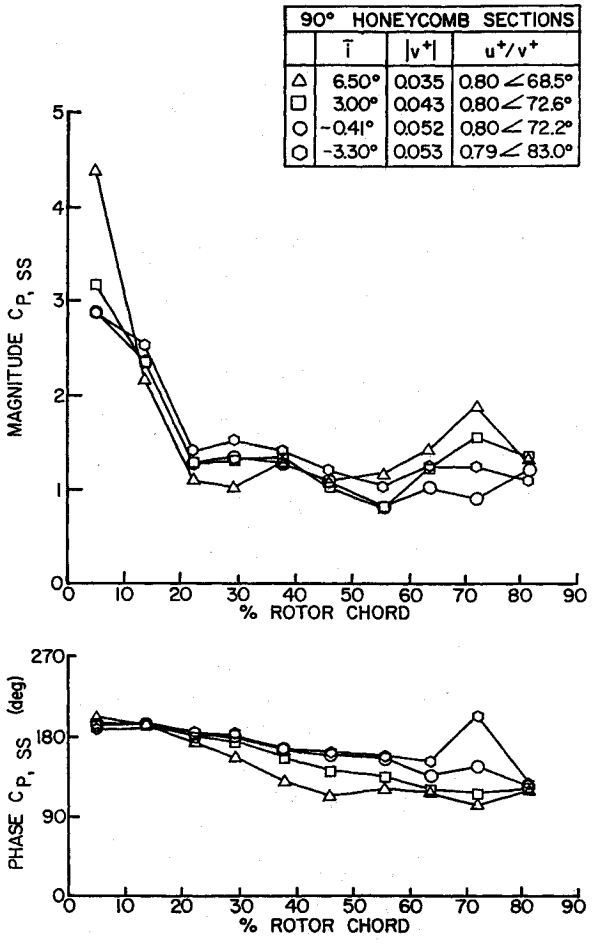

Fig. 11 Suction surface 90-deg honeycomb attached flow generated gust response.

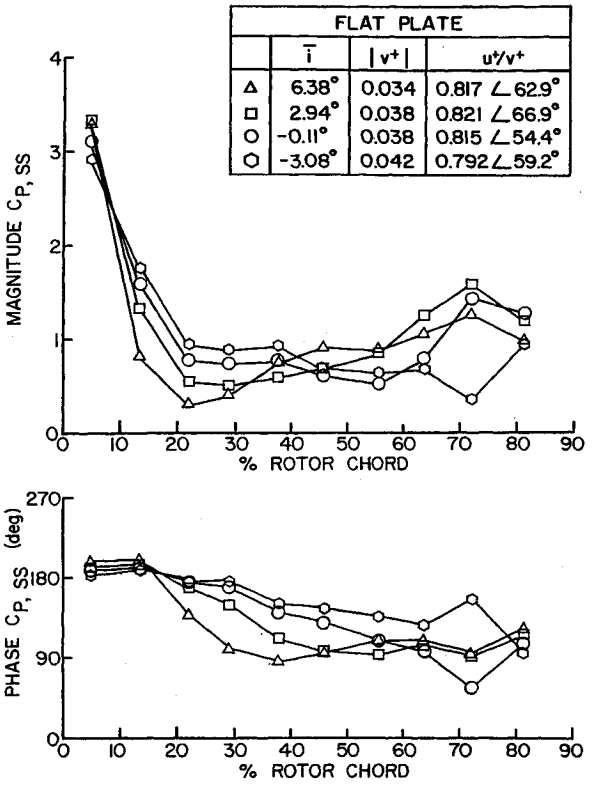

Fig. 12 Suction surface flat plate separated flow generated gust response.

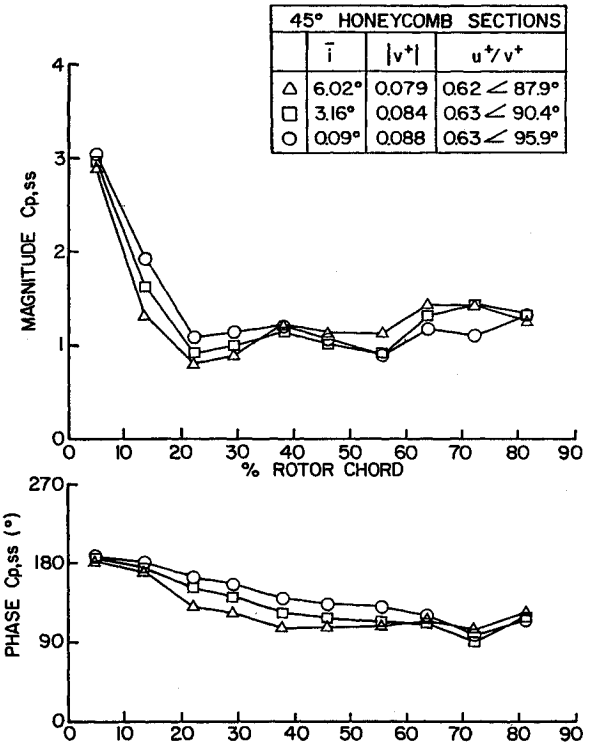

Fig. 13 Suction surface 45-deg honeycomb separated flow generated gust response.

loading at approximately 20% chord for flow incidence angles of 3 and 6 deg. There is also a rapid increase and decrease in the gust phase response at 65% chord for the −3-deg flow incidence. The suction surface gust phase response from the flat plate and the 45-deg honeycomb forcing functions are very similar to that generated by the 90-deg honeycomb attached flow, but the steady loading dependence occurs at all levels (Figs. 12 and 13). These gust phase responses differ

from those resulting from the airfoil generated separated flow in that the chordwise position at which the large phase decrease starts moves forward.

As compared to the attached and separated flow generated suction surface responses of Kim and Fleeter,[9] the chordwise trends in the suction surface response are similar for the magnitude data, but different for the phase data. Thus, the suction surface gust response magnitude appears to be less sensitive to the particular forcing function generator than the pressure surface gust response for both attached and separated flow forcing functions.

Unsteady Pressure Difference

As expected, based on the individual airfoil surface data, changes in the gust generator flowfield has a significant effect on the unsteady pressure difference. Figures 14–16 show the pressure difference gust response resulting from the 90-deg honeycomb attached flow forcing function, flat plate separated flow forcing function, and the 45-deg honeycomb separated flow forcing function. The pressure difference magnitude data decrease with chord, with the decrease in the leading-edge region being more rapid as the flow becomes separated and with increased steady loading. This results in good agreement between the attached flow 90-deg honeycomb generated pressure difference magnitude data and the linear theory prediction, with the agreement decreasing for the separated flow forcing function generated responses due to the flat plates and the 45-deg honeycombs.

The resulting gust pressure difference phase from the 90-deg honeycomb attached flow forcing function is independent of chord over the front 40% chord, becoming a strong function of steady loading, increasing in value with loading and chordwise position. The phase data are in poor agreement with theory, with the sudden increase in phase in the aft chord region not predicted by theory. When the forcing function flowfield is changed to separated flow, significant changes occur. Note that the gust phase responses due to the flat plate and 45-deg honeycomb separated flow forcing functions are nearly identical (Figs. 14 and 15). Unlike the attached flow generated response, the phase response increases with chord and steady loading over most of the chord. However, the

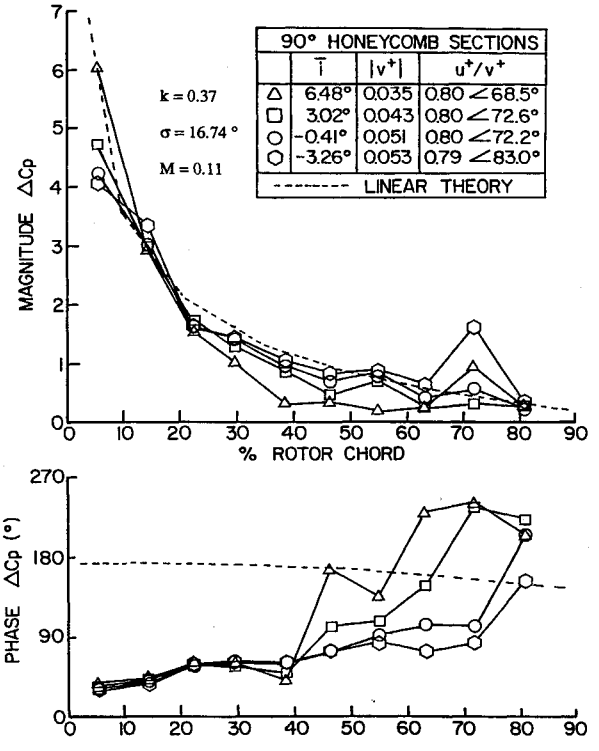

Fig. 14 Pressure difference 90-deg honeycomb attached flow generated gust response.

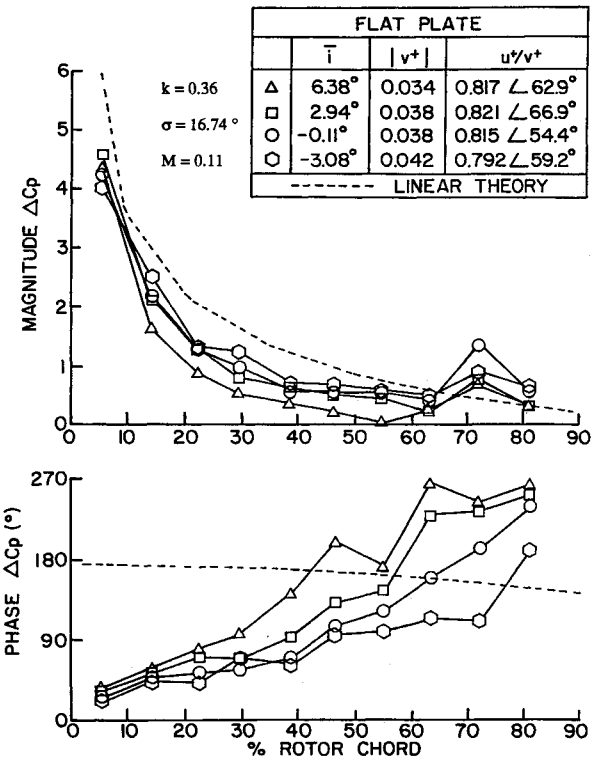

Fig. 15 Pressure difference flat plate separated flow generated gust response.

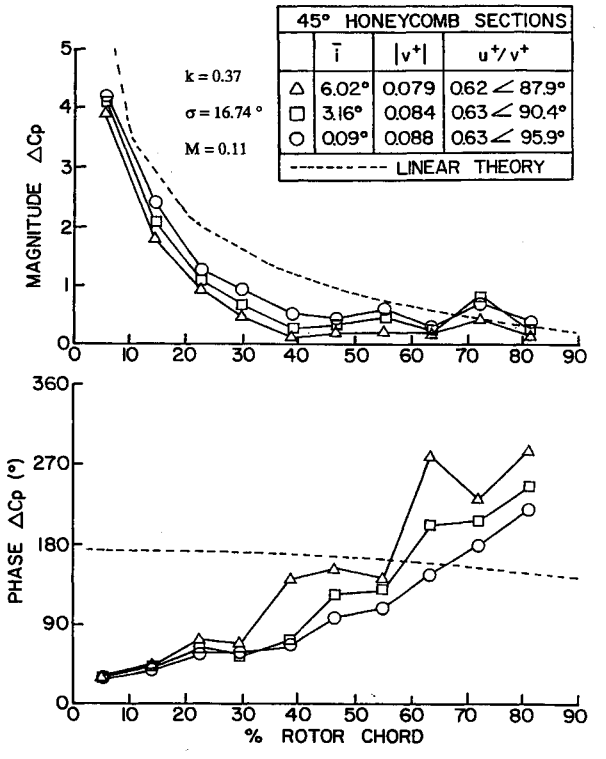

Fig. 16 Pressure difference 45-deg honeycomb separated flow generated gust response.

pressure difference phase data from the separated flow forcing functions are also in poor agreement with the linear theory predictions for both separated flow forcing functions.

These results, combined with those of the NACA airfoil generated responses, show that the unsteady pressure difference resulting from different gust generators with attached flow have similar magnitude data trends, but not necessarily phase data trends. For separated flow generated forcing func-

tions of different gust generators, the responses have similar trends in both magnitude and phase. These differences in the pressure difference gust response among different gust generators are similar to those seen on the suction surface. This suggests that the suction surface gust response is dominant over the pressure surface gust response. Also, in general, the pressure and suction surface and the pressure difference responses resulting from attached flow forcing functions are more sensitive to the gust generator than the corresponding gust responses generated by separated forcing functions.

Unsteady Lift Correlation with Linear Theory

The deviation of the differential pressure coefficient data from the linear theory prediction is quantified through the unsteady lift coefficient ratio L_{corr}. Figure 17 shows the variation of L_{corr} with the mean flow incidence angle. The NACA 0024 airfoil generated data of Kim and Fleeter[9] are also shown in these figures for comparison. In regard to the magnitude correlation, the 90-deg honeycomb attached flow generated forcing function correlates much better than the separated flow generated forcing functions—the flat plates and the 45-deg honeycombs.

These data further support the influence of forcing function flow separation on decreased correlation with linear theory, discovered by Kim and Fleeter.[9] Furthermore, the effect of decreased magnitude correlation with steady loading is clearly evident in the nearly linear way in which the 90-deg honeycomb, flat plate, and the 45-deg honeycomb forcing function generated data correlation decreases with steady loading. These results are possible with the honeycombs and flat plates because the magnitude of the gust ratio, u^+/v^+ could be controlled, which was not possible with the NACA 0024 airfoils. The pressure difference phase correlation with linear theory is unaffected by the forcing function fluid dynamics, i.e., attached or separated flow.

Forcing Function Fundamental Parameters

To begin to understand the fundamental differences between the response data generated by the attached and separated flow and the correlation of these data with linear theory, the validity of the unsteady linear theory model for these flows is considered. In particular, as considered by Henderson and Fleeter,[11,12] linear theory requires that 1) the vortical gust vector components u^+ and v^+ are 180 deg out of phase; 2) the magnitude of u^+/v^+ is equal to the ratio k_2/k_1, determined from the steady flow velocity triangle; 3) the vortical gust vector is perpendicular to the direction of gust convection; and 4) the vortical gust vectors are parallel to one another. Note the presence of these features in the linear theory vortical gust, shown in Figure 18. When assumptions 1 and 2 are valid, the gust automatically satisfies assumptions 3 and 4. However, if these assumptions are not satisfied, the character of the vortical gust changes in the manner shown in Fig. 18. When the phase angle requirement is violated, the gust vectors become nonperpendicular to the direction of gust convection, whereas when the wave number ratio to gust magnitude ratio equivalency is violated, the gust vectors become nonparallel.

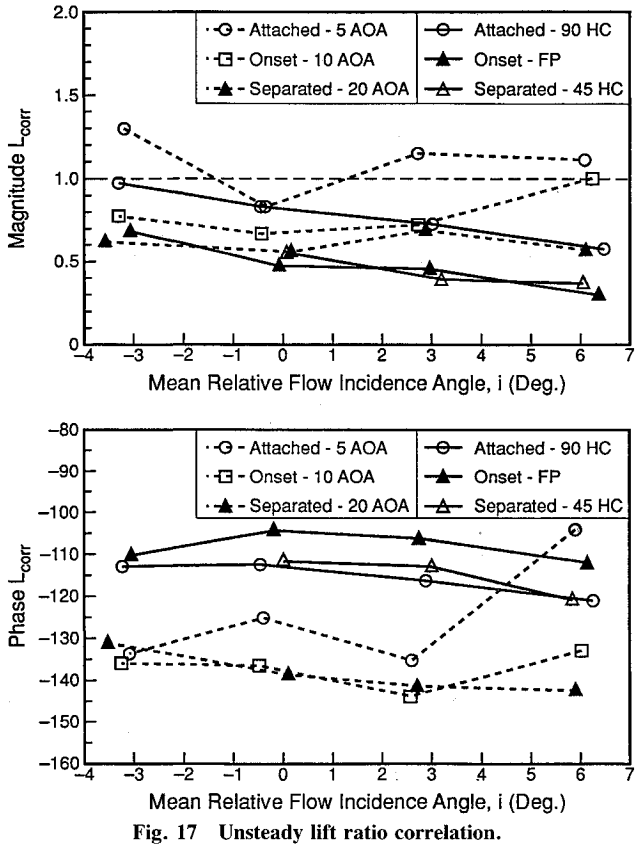

Fig. 17 Unsteady lift ratio correlation.

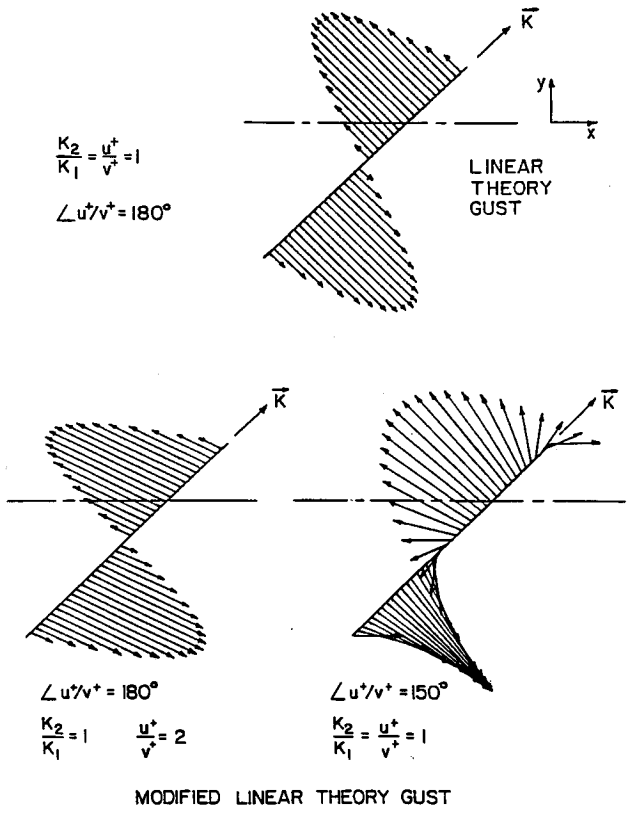

Fig. 18 Linear theory gust.

The importance of the gust ratio phase angle with regard to the applicability of linear theory to turbomachine blade rows is illustrated by the consideration of the first linear theory assumption: the streamwise and transverse vortical gust components, u^+ and v^+, are 180 deg out of phase. This assumption is violated independent of whether the forcing function gusts are generated by separated or attached flows. For all of the experiments, the phase of u^+/v^+ was generally near 70 deg. The significance of the gust ratio phase parameter for the pressure difference phase data-theory correlation is evident in Fig. 19, which shows L_{corr} as a function of the gust ratio phase. Note that the honeycomb and flat plate generated phase data, along with the 5-deg AOA 6-deg incidence NACA 0024 airfoil generated phase data with a gust ratio phase equal to 54 deg, correlate significantly better than the other NACA 0024 airfoil generated phase data, having gust ratio phase angles less than 32 deg. Hence, the violation of the 180-deg phase requirement is an important factor in the correlation of the pressure difference phase data with linear vortical gust theory.

Table 2 Unsteady $|u^+/v^+|$ and steady flow k_2/k_1 values

Steady loading, $\bar{\imath}$		−3 deg	0 deg	3 deg	6 deg
Forcing functions					
Attached flow (90-deg honeycombs)	$\lvert u^+/v^+\rvert$	0.787	0.802	0.797	0.800
	k_2/k_1	0.288	0.230	0.201	0.150
	% Difference	173%	249%	297%	433%
Separated flow (flat plates)	$\lvert u^+/v^+\rvert$	0.792	0.815	0.821	0.817
	k_2/k_1	0.300	0.250	0.124	0.104
	% Difference	168%	226%	562%	686%
Separated flow (45-deg honeycombs)	$\lvert u^+/v^+\rvert$	——	0.634	0.628	0.620
	k_2/k_1	——	0.232	0.176	0.121
	% Difference	——	173%	257%	412%

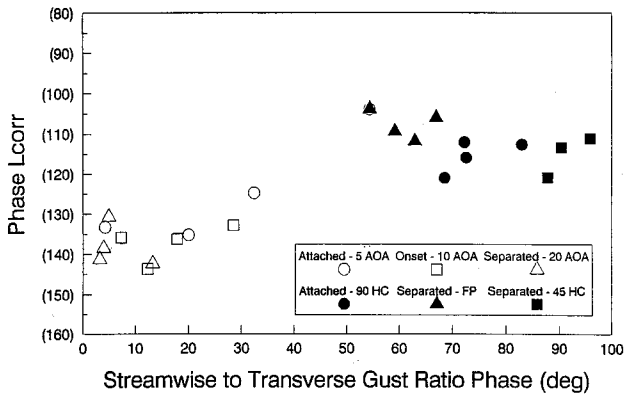

Fig. 19 Unsteady lift ratio variation with gust component ratio.

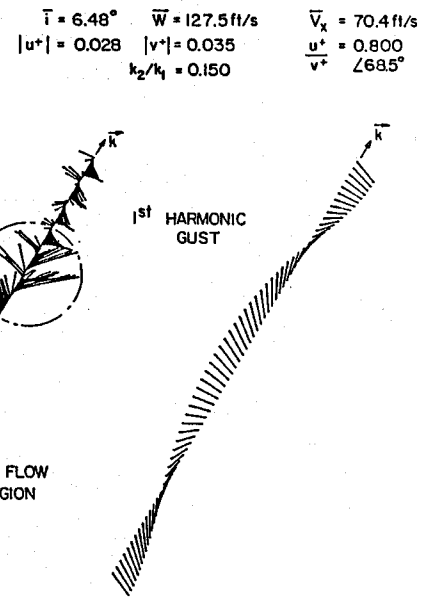

Fig. 20 90-deg honeycomb attached flow generated unsteady aerodynamic gust.

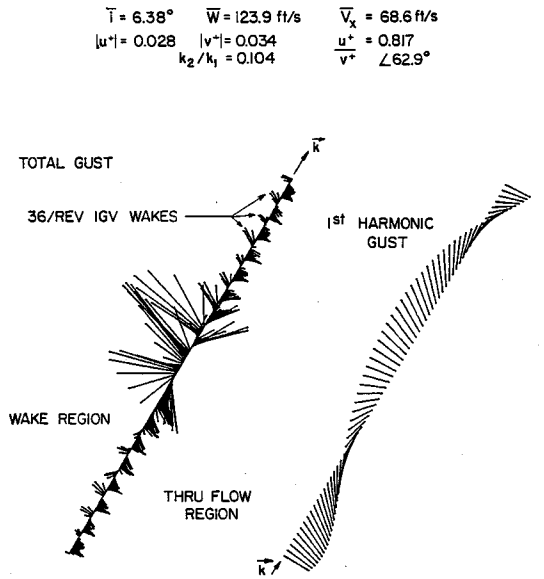

Fig. 21 Flat plate separated flow generated unsteady aerodynamic gust.

Linear theory also requires the magnitude of the vortical gust component ratio u^+/v^+ be equal to the ratio k_2/k_1, the wave number ratio calculated from the steady velocity data. This assumption is grossly violated as evident in Table 2. There is not a single case for which the two values agree. In fact, the unsteady u^+/v^+ values are 2–5 times greater than that of the steady k_2/k_1 values.

The effect of violating the above assumptions on the unsteady aerodynamic gust may be reflected in the interesting trend apparent in the first harmonic gust vectors. These gust vectors represent the spatial distribution of the forcing function aerodynamic gust vector, ΔW, in the direction of gust convection. This spatial distribution of the gust vector is constructed by plotting the temporal variations in ΔW spatially in the direction of gust convection, with the magnitude and direction with respect to k maintained. The maximum magnitude of the first harmonic gust vectors from the 90-deg honeycomb attached flow (Fig. 20), the flat plate separated flow (Fig. 21), and the 45-deg honeycomb separated flow (Fig. 22) are all in the midwake and midthrough flow regions. Thus, the gust vectors form a shape that is somewhat sinusoidal. In particular, note the symmetry of the 45-deg honeycomb first harmonic gust vectors with the largest gust ratio phase angle of 87.9 deg (Fig. 22). Kim and Fleeter[9] had discovered that the gust shapes were skewed-sinusoids when the gust phase angles were near zero. Thus, the first harmonic gust vectors are influenced significantly by the gust ratio phase angle, independent of the forcing function fluid dynamics. This supports the findings of Kim and Fleeter that the gust ratio phase angles closer to 180 deg produce wakes that resemble more the linear theory gust.

The prevalence of the sinusoid shape for these three gust vectors, despite the different levels of discrepancy between the magnitude of u^+/v^+ and k_2/k_1, support the findings of Kim and Fleeter[9] that the gust ratio phase angle is the dominant factor in the gust shape determination than the matching of u^+/v^+ magnitude to k_2/k_1.

The violation of the first two assumptions leads to the violation of the last two assumptions, resulting in gust vectors which are neither parallel to one another nor perpendicular to the direction of wake convection. The assumptions of perpendicularity between the vortical gust vectors and the di-

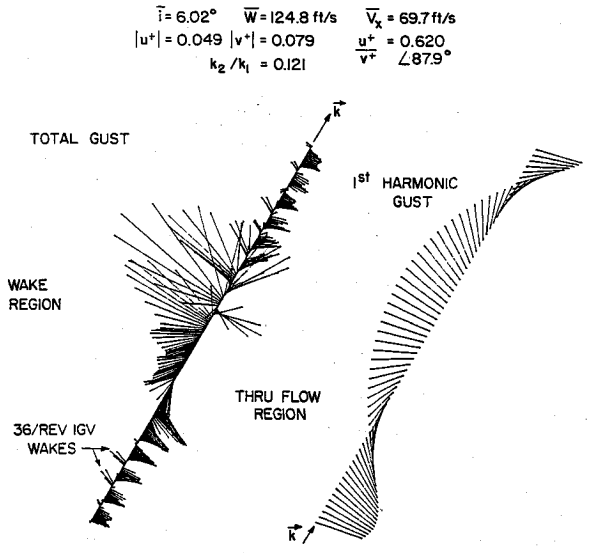

Fig. 22 45-deg honeycomb separated flow generated unsteady aerodynamic gust.

rection of the vortical gust convection $\boldsymbol{k}$ are clearly inappropriate, as demonstrated in Figs. 18–20 which show the honeycomb and flat plate generated total and first harmonic gust vectors that are convected over the rotor blade. Note that few, if any, of the vectors in the total gust are perpendicular to the direction of convection. In fact, what is evident is a fanning out trend of the vectors in the wake region that increases with increased forcing function flow separation. Note, in all these cases, the 36/rev IGV wakes are embedded within the larger 2/rev NACA airfoil wake in the total gust. The 2/rev total gust vectors from the 90-deg honeycomb attached flow differ from those of the 5-deg AOA airfoil with attached flow, with the 2/rev gust vectors of the honeycombs crossing only in the edges of the wake region, shown as circled regions in Fig. 20, but fan in the wake region. However, this fanning may be due to the IGV wakes since the total gust magnitudes of the IGV are of the same order of magnitude as the honeycomb total gust magnitude. The total gust vectors from the separated flow plate and 45-deg honeycomb (Figs. 21 and 22) continuously fan over the entire wake region. In summary, the total gust vectors are not perpendicular to the direction of gust convection, nor are they parallel to one another. For most wake generators, regardless of type, the gust vectors start being crossed with attached flow and fan with increased separation, with the fanning being particularly wide for more separated flows. These results indicate that the total forcing function gust vectors are largely affected by the forcing function fluid dynamics, in contrast to the first harmonic gust vectors.

Therefore, the consideration of some essential assumptions inherent in the unsteady linear vortical gust theory indicate that these assumptions are not appropriate for turbomachine blade rows and cannot be applied. The poor data-theory correlation of the resulting blade row unsteady aerodynamic response suggests an intimate relationship between the characteristics of the gust vector and the degree of correlation of the compressor blade row unsteady aerodynamic gust response data with linear theory. Current models do not incorporate the specific details of the gust such as the gust ratio phase angle. Instead, since certain characteristics are inherent in the current linear theory model, any deviation from these characteristics would contribute to an error in the prediction value of the unsteady aerodynamics. Hence, advancements in the gust modeling technique to include parameters, such as the gust ratio phase angle, the gust ratio magnitude, and potential effects are critical to improving the ability to predict blade unsteady pressure response.

Summary and Conclusions

A series of experiments were performed to investigate the fundamental forcing function phenomena fluid dynamics generating different blade row gust responses in a controlled manner, including the important effects associated with the forcing function gust magnitude. This was accomplished through the investigation of unsteady aerodynamic blade row response to gusts generated by attached and separated flow fluid dynamics from nonairfoil shape gust generators. With these gust generators, the gust ratio magnitude can be controlled without affecting the forcing function fluid dynamics, i.e., attached or separated flow, thereby enabling a controlled study of the effect of steady loading.

These experiments clearly show that the forcing function generator fluid dynamics is significant with regard to the resulting unsteady aerodynamic gust response of a downstream airfoil row, while enabling a controlled study of the effect of steady loading for the first time. The applicability of the concept of attached and separated flow forcing functions and the resulting unsteady aerodynamic response is broadened over previous data[9] to include nonairfoil shape gust generators. It was shown that although differences in the individual surface responses occur, gust generator flowfields can be broadly categorized into attached or separated flow forcing functions, with the resulting gust response correlation with linear theory models predictable. In particular, the attached flow and separated flows generate large and important differences in forcing function characteristics and the resulting unsteady aerodynamic blade row gust response, such that the correlation with linear theory decreases with increased forcing function flow separation. Steady loading is found to linearly decrease the unsteady aerodynamic pressure difference data-theory correlation.

The forcing function fluid dynamics was analyzed in terms of the requirements inherent in the linear theory vortical gust modeling. This showed that the forcing function violation of the 180-deg phase requirement between the streamwise and transverse gust components contributed to the poor data-theory phase correlation, and that the addition of the values of $|u^+/v^+|$ and k_2/k_1 not being equal leads to unsteady gust vectors which are neither parallel to one another nor perpendicular to the direction of wake convection, as also inherent in linear theory vortical gust models. Thus, the degree of correlation of the rotor blade unsteady gust response data with linear theory is closely related to the characteristics of the forcing function gust generating the response.

Acknowledgment

Research was sponsored by the Air Force Office of Scientific Research (AFSC) under Contract F49620-88-C-0022.

References

[1]Whitehead, D. S., "Classical Two-Dimensional Methods," *AGARDograph No. 298, AGARD Manual on Aeroelasticity in Axial Flow Turbomachines, Volume 1: Unsteady Turbomachinery Aerodynamics*, pp. 3.1–3.30.

[2]Fleeter, S., "The Fluctuation Lift and Moment Coefficients for Cascaded Airfoils in a Nonuniform Compressible Flow," *Journal of Aircraft*, Vol. 10, No. 2, 1973, pp. 93–98.

[3]Adamczyk, J. J., and Goldstein, M. E., "Unsteady Flow in a Supersonic Cascade with Subsonic Leading Edge Locus," *AIAA Journal*, Vol. 16, No. 12, 1978, pp. 1248–1254.

[4]Verdon, J. M., and Usab, W. J., "Application of a Linearized Unsteady Aerodynamic Analysis to Standard Cascade Configurations," American Society of Mechanical Engineers Paper 90-GT-11, June 1990.

[5]Verdon, J. M., and Hall, K. C., "Development of a Linearized Unsteady Aerodynamic Analysis for Cascade Gust Response Predictions," NASA Rept. 4308, July 1990.

[6]Scott, J. S., and Atassi, H. M., "Numerical Solutions of the Linearized Euler Equations for Unsteady Vortical Flows Around Lifting Airfoils, AIAA Paper 90-0694, Jan. 1990.

[7]Fang, J., "Compressible Flows with Vortical Disturbances Around Cascades of Airfoils," Ph.D. Dissertation, Univ. of Notre Dame, Notre Dame, IN, April 1991.

[8]Manwaring, S. R., and Fleeter, S., "Forcing Function Effects on Rotor Periodic Aerodynamic Response," *Journal of Turbomachinery*, Vol. 113, No. 2, 1991, pp. 312–319.

[9]Kim, K. H., and Fleeter, S., "Compressor Blade Row Unsteady Aerodynamic Response to Attached and Separated Flow Forcing Functions," AIAA Paper 92-0147, Jan. 1992.

[10]Smith, S. N., "Discrete Frequency Sound Generation in Axial Flow Turbomachines," Aeronautical Research Council R&M 3709, Great Britain, UK, March 1972.

[11]Henderson, G. H., and Fleeter, S., "Forcing Function Effects on Unsteady Aerodynamic Gust Response: Part I Forcing Functions," American Society of Mechanical Engineers Paper 92-GT-174, June 1992.

[12]Henderson, G. H., and Fleeter, S., "Forcing Function Effects on Unsteady Aerodynamic Gust Response: Part II Low Solidity Airfoil Row Response," American Society of Mechanical Engineers Paper 92-GT-175, June 1992.